Journal of Fluids and Structures 17 (2003) 1043–1058

JOURNAL OF FLUIDS AND STRUCTURES

www.elsevier.nl/locate/jnlabr/yjfls

# Flow structure around two finite circular cylinders located in an atmospheric boundary layer: side-by-side arrangement

C.W. Park[a], S.J. Lee[b,*]

[a] *School of Mechanical Engineering, Kyungpook National University, Daegu 702-701, South Korea*
[b] *Department of Mechanical Engineering, Pohang University of Science and Technology, Pohang 790784, South Korea*

Received 9 July 2002; accepted 24 March 2003

**Abstract**

The flow structure around the free-end region of two adjacent finite circular cylinders embedded in an atmospheric boundary layer (ABL) was investigated experimentally. The experiments were carried out in a closed-return-type subsonic wind tunnel, in which two finite cylinders with an aspect ratio of 6 were mounted vertically on a flat plate in a side-by-side arrangement. The Reynolds number based on the cylinder diameter was about $Re = 2 \times 10^4$. Systems with gap ratios (i.e., center-to-center distance/cylinder diameter) in the range 1.0–2.0 were investigated. A hot-wire anemometer was employed to measure the wake velocity, and the mean pressure distribution on the cylinder surface was also measured. The flow past two finite cylinders was found to have a complicated three-dimensional wake structure in the region near the free ends. As the gap ratio increases, regular vortex-shedding becomes dominant, but the length of the vortex formation region decreases. The pressure distribution and flow structure around two cylinders were found to differ substantially from the behavior of a two-dimensional circular cylinder due to mutual interference. The three-dimensional flow structure seems to originate from the strong entrainment of irrotational fluids caused by the downwash counter-rotating vortices separated from the finite cylinder (FC) free ends.


## 1. Introduction

Fluid flow past a circular cylinder has been examined in numerous experimental studies due to its simple geometry and coherent vortex structure. These studies have generated large amounts of data on properties such as the surface pressure, drag coefficient and vortex-shedding. The circular cylinder has attracted particular attention because it can be looked upon as a representative bluff body and because it shows two-dimensional flow characteristics. However, it is well known that the wake behind a two-dimensional body placed in a uniform flow is rarely two-dimensional, even at Reynolds numbers that are sufficiently low for the vortex street to be present. The three-dimensionality of the cylinder wake manifests as characteristics such as slantwise shedding, irregular waviness, and bowed vortices. Slaouti and Gerrard (1981) reported that the wake behind a cylinder is two-dimensional at Reynolds numbers less than about 80. In general, the degree of three-dimensionality increases with increasing Reynolds number.

In the near-wake just behind a two-dimensional circular cylinder, however, the three-dimensionality is weak because the vortex-shedding is regular and parallel to the cylinder axis. Therefore, the cylinder wake has been assumed to be a two-dimensional flow in view of its coherent structure, in which the Strouhal number is constant along the cylinder axis when appropriate end plates are attached (Szepessy and Bearman, 1992).

*Corresponding author. Tel.: +82-54-279-2169; fax: +82-54-279-3199.
*E-mail address:* sjlee@postech.ac.kr (S.J. Lee).

0889-9746/03/$ - see front matter 
doi:10.1016/S0889-9746(03)00070-7

Many real-world bluff bodies such as tall buildings cannot be modelled as a two-dimensional (2-D) bluff body like the infinite cylinder, but can be modelled as a finite cylinder (FC) with a free end. As a result, the study of a FC embedded in an atmospheric boundary layer (ABL) flow is of interest because of its importance to civil and wind engineering applications (Uematsu et al., 1990; Fox et al., 1993). In order to properly design high-rise structures such as tall buildings and cooling towers, the wind loading and flow-induced oscillations of the structure should be considered in the design process. The presence of the free end changes the flow structure in the near-wake region, including the characteristics of the vortex formation region, the vortex-shedding pattern and the surface pressure distribution. The three-dimensionality of the cylinder wake is caused by numerous factors, such as the nonuniformity of the free-stream flow, the presence of longitudinal secondary vortices, and the low aspect ratio of the cylinder. In particular, the free end of a FC acts as a direct and significant source of three-dimensionality.

In the region near the base of a three-dimensional (3-D) bluff body, an adverse pressure gradient is formed due to deflection of flow by the obstacle. In addition, one or more vortices are induced and stretched into a horseshoe shape. Many studies have examined the horseshoe vortex that forms around the base of a 3-D bluff body (Castro and Robins, 1977; Sakamoto and Arie, 1983). Another important feature of flow around a 3-D finite bluff body is flow separation from the top and side surfaces. Williamson (1989) found a discontinuity in the Strouhal–Reynolds number relationship and oblique vortex-shedding at low Reynolds numbers. He attributed the discontinuity in the Strouhal–Reynolds number relationship to the transition from one oblique vortex-shedding mode to another. In addition, he found that the critical Reynolds number depended on the flow nonuniformity, end conditions, and the level of free-stream turbulence.

Baban and So (1991) found that the fluctuating re-circulating flow behind the finite cylinder was the flow mechanism responsible for the unsteady drag and caused it to increase beyond the fluctuating lift. This was attributed to the unsteady turbulent shear flow separated from the free end of the FC. Okamoto and Sunabashiri (1992) found that the wake behind finite cylinders of small aspect ratio ($L/D=1$–$2$) is symmetric, but that the wake pattern becomes three-dimensional when the aspect ratio exceeds $L/D=4$. Farivar (1981) investigated the effect of a FC free end on flow characteristics by measuring the mean pressure, pressure fluctuations and drag force acting on finite cylinders of various aspect ratios exposed to a uniform flow. He found that regular vortex-shedding disappeared for aspect ratios smaller than $L/D=7.5$.

Sayers (1988) measured the lift and drag forces acting on a single cylinder in a group of four 2-D cylinders situated in a uniform flow, and found that the forces varied greatly with changes in the spacing ratio and inclination angle. Sitheeq et al. (1997) investigated the effect of integral length scale on the surface pressure distribution of a 3-D square prism located in an ABL. Sumner et al. (1999) used the particle image velocimetry (PIV) velocity field measurement technique to measure the flow field at low Reynolds numbers around groups of two or three circular cylinders of equal diameter arranged in a side-by-side configuration. They found that the two-cylinder arrangement typically gives rise to two vortex streets that are synchronized in an anti-phase or in-phase fashion. Mahir and Rockwell (1996) studied the vortex formation behind two cylinders subjected to forced excitation over a wide range of frequencies and phase angles.

Williamson (1985) investigated the flow behind a pair of 2-D circular cylinders in a side-by-side arrangement using various flow visualization methods. He found that either in-phase or out-of-phase vortex-shedding synchronization occurred when the gap size between the two bodies was increased beyond a critical value. Additionally, the flow became asymmetric when the gap was smaller than this critical gap size. Sun et al. (1992) investigated the pressure fluctuations on two circular cylinders at high Reynolds numbers for various arrangements of the cylinders with respect to the flow. The interference effect on the fluctuating surface pressure was weaker at supercritical Reynolds numbers than at subcritical ones.

Most previous studies have examined two-dimensional bluff bodies located in a uniform flow. However, the flow behind two or more three-dimensional bluff bodies embedded in an atmospheric boundary layer (ABL) has yet to be fully investigated. The main objectives of the present study were to investigate the effect of the gap distance between two finite cylinders embedded in ABL on the flow characteristics of the near-wake and to elucidate the flow structure near the FC free end in detail.

## 2. Experimental apparatus and methods

### 2.1. Hot-wire anemometry and flow visualization

The experiments were performed in a closed-return-type subsonic wind tunnel with a test-section of 0.72 ($W$) × 0.6 ($H$) × 6 ($L$) m. Spires and roughness elements were installed in front of the test-section to generate a neutrally buoyant ABL. Artificial lawn of height 10 mm was installed along the streamwise direction behind the spires to simulate the ABL over open terrain. The reference velocity at the end of the FC was fixed at $U_0=10$ m/s and the corresponding Reynolds

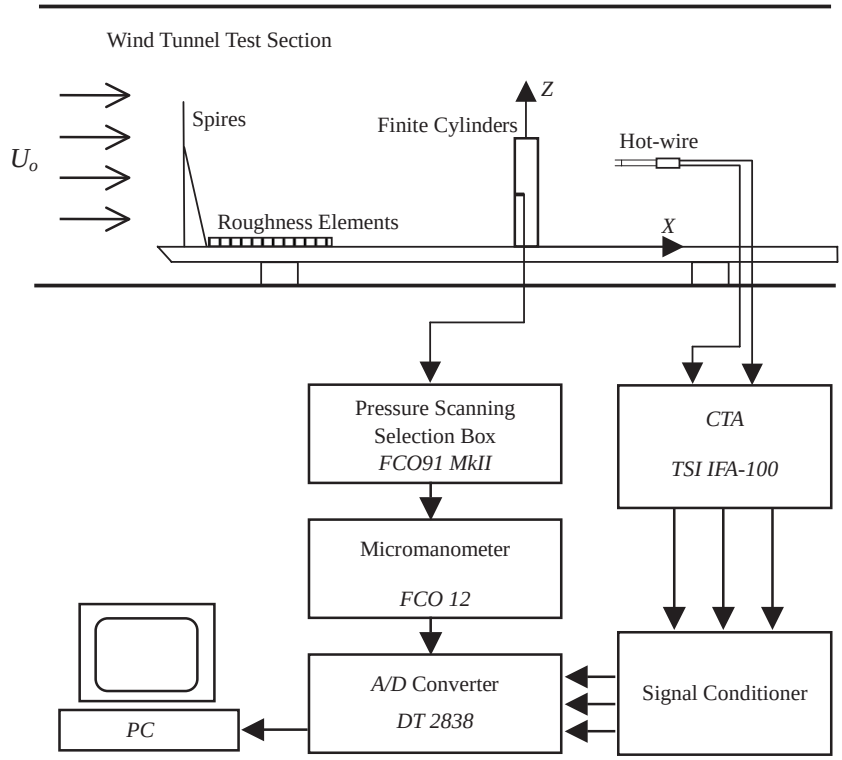


Fig. 1. Wind tunnel test section and flow measurement system.

number based on the cylinder diameter ($D = 30$ mm) was about $\mathrm{Re} = 2 \times 10^4$. The FC was installed vertically on a 15-mm-thick flat plate with a sharp leading edge of angle 30°, which was separated 57 mm from the bottom surface of the wind tunnel. The FC model was located 3.9 m downstream from the leading edge of the flat plate. A schematic diagram of the wind tunnel test-section and flow measurement system is given in Fig. 1.

The velocity profiles of the simulated ABL were measured using a hot-wire anemometer. The mean velocity and turbulence intensity profiles of the streamwise velocity component measured at the location of the FC model ($X = 0$) are shown in Fig. 2. The mean streamwise velocity profile in the ABL follows a power law of the form:

$$U(Z)/U_0 = (Z/L)^n, \tag{1}$$

where $U_0$ is the reference velocity and $L$ is the height of the FC. The velocity profile of the simulated ABL, which corresponds to the atmospheric velocity profile over open terrain, is well fitted by $n = 0.14$ (Simiu and Scanlan, 1996). The thickness of boundary layer developed on the bottom plate was about 21.3 cm at the FC location. In a previous study (Park and Lee, 2002), we investigated the effects of oncoming velocity profile and boundary layer thickness on the flow structure around a single surface-mounted finite cylinder.

For this kind of wind engineering experiment, the simulated ABL should reproduce not only the mean velocity and turbulence intensity profiles, but also the power spectrum of the streamwise velocity component. The integral length scale ($L_u^x$) of oncoming boundary layer flow can be estimated using the autocorrelation of the longitudinal wind velocity fluctuations, assuming that Taylor's hypothesis is valid. From Taylor's hypothesis, the integral length scale is defined as

$$L_u^x = \bar{U} T_u, \tag{2}$$

where $\bar{U}$ is the streamwise mean flow speed, and the integral time scale $T_u$ is given by

$$T_u(z) = \int_0^\infty R_u(z, \tau)\, \mathrm{d}\tau. \tag{3}$$

Here, $\tau$ is the time lag and $R_u$ is the autocorrelation function, which is defined as

$$R_u = u(t)u(t + \tau)/\sigma_u^2, \tag{4}$$

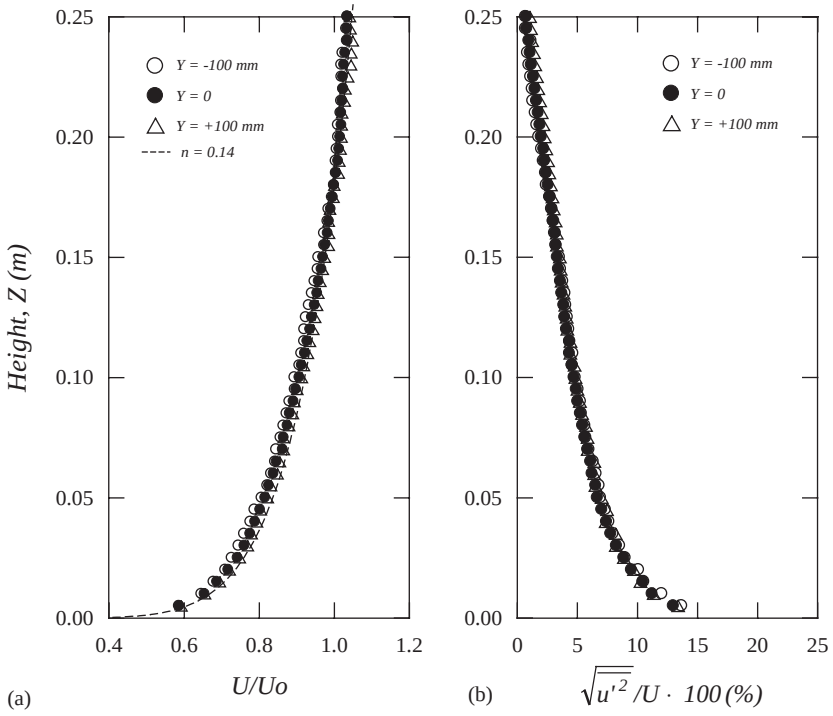


Fig. 2. Streamwise mean velocity and turbulence intensity profiles of atmospheric boundary layer measured at the location of finite cylinder ($X=0$): (a) mean velocity; (b) turbulence intensity.

where $\sigma_u$ is the root mean square (r.m.s.) value of the streamwise velocity component $u$. In the strict sense, all of these parameters should be simulated in the wind tunnel. Unfortunately, there is considerable scatter in the values of the real atmospheric parameters. In a previous study using the same wind tunnel, we found that the integral length scale calculated from the wind tunnel data ranged from 32 to 59 cm (Park and Lee, 2002).

Fig. 3 shows the power spectral density (PSD) distribution of the longitudinal velocity component of the oncoming ABL over open terrain at the height of $Z=0.25$ m. The von Kármán spectrum can be written as

$$\frac{nS_u(z,n)}{\sigma_u^2} = 4\,\frac{nL_u^x}{\bar{U}}\Big/\left[1+70.8\left(\frac{nL_u^x}{\bar{U}}\right)^2\right]^{5/6}, \tag{5}$$

where $S_u(z,n)$ is the power spectral density of the longitudinal flow velocity at frequency $n$ (Simiu and Scanlan, 1996). As shown in Fig. 3, the nondimensional power spectral density distribution matches well with the von Kármán spectrum. This indicates that the ABL simulated in the wind tunnel is kinematically similar to full-scale natural wind.

The FC was made of stainless steel rod and its surface was sandpapered smooth. For the side-by-side arrangement, two finite cylinders with the same aspect ratio of $L/D=6$ were used to investigate the effect of the gap ratio ($G/D$) on the flow characteristics. The gap ratio ($G/D$) is defined as the ratio of the center-to-center distance $G$ between two cylinders to the cylinder diameter $D$. In order to avoid flow-induced structural vibrations, the natural frequency of the FC model was set to be greater than 20 times the vortex-shedding frequency (Baban and So, 1991). It is possible that a horseshoe vortex formed at the junction of the FC model and the ground plate; however, the present study focused on the flow structure near the free end of the FC, and all experimental measurements were performed in the region between mid-height and the FC free end. Therefore, the effect of a horseshoe vortex near the ground is unimportant and beyond the scope of this study (Okamoto and Sunabashiri, 1992; Park and Lee, 2002).

In this study, the gap ratio ($G/D$) was varied from 1.0 to 2.0 in intervals of 0.25 to investigate in detail the flow pattern arising from the deflection of gap flow. The gap ratio of $G/D=2.0$ is known to be a critical value above which the flow field recovers its symmetry and sustains regular vortex-shedding, and numerous studies have been made of systems with gap ratios in the range $2<G/D<6$ (Williamson, 1985; Sumner et al., 1999; Bearman and Wadcock, 1973; Spivack,

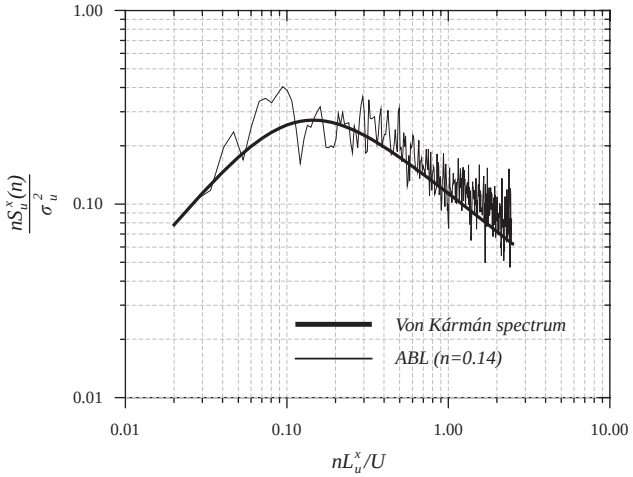


Fig. 3. Power spectral density of longitudinal velocity component at $Z=0.25\,\mathrm{m}$ ($U_0=10\,\mathrm{m/s}$).

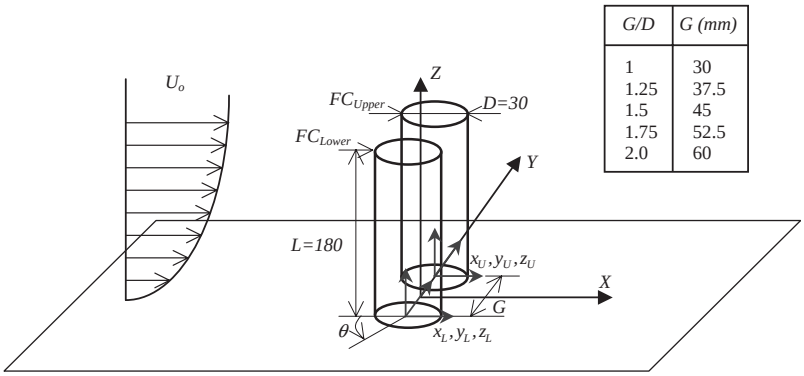


| G/D | G (mm) |
|---|---|
| 1 | 30 |
| 1.25 | 37.5 |
| 1.5 | 45 |
| 1.75 | 52.5 |
| 2.0 | 60 |

Fig. 4. Finite cylinder models and coordinate systems (unit:mm).

1946). Therefore, in the present study we focused on gap ratios smaller than the critical value, including the no-gap condition ($G/D=1.0$). Three independent geometrical coordinate systems (upper cylinder, lower cylinder and center of gap) were used for a better understanding of the flow structure. The FC models and coordinate system used in this study are shown in Fig. 4.

The wake velocity was measured using I-type and X-type hot-wire probes connected to a constant temperature hot-wire anemometer (TSI IFA 100). The hot-wire probe was traversed to the measuring points using a 3-D traverse with an accuracy of 10 μm. At each measurement point, 32 000 data were acquired at a sampling rate of 2 kHz after low-pass filtering at 800 Hz. During the experiments, the temperature variation in the wind tunnel test-section was maintained at less than 0.5°C. West and Apelt (1982) found that the pressure distribution around a circular cylinder varies only slightly with respect to the blockage ratio. For blockage ratios less than 6%, the Strouhal number is independent of the blockage ratio and cylinder aspect ratio. Since the maximum blockage ratio for the two-FC models considered here was about 3%, the blockage effect was not considered in the present study.

To visualize the flow field around the FC free end, a particle tracer method was employed in a circulating water channel of test-section 0.3 ($W$) × 0.2 ($H$) × 1.2 ($L$) m. The free stream velocity was fixed at 12 cm/s and an ABL almost the same as that of the wind tunnel tests was simulated in the circulating water channel. Polyvinylchloride particles of average diameter 100 μm were seeded as tracer particles. The particle pathlines near the FC free end were illuminated with a thin cold light sheet, emitted from a 150 W halogen lamp. Images of the scattering from the particles were photographed with a Nikon *F5* camera.

### 2.2. Pressure measurement system

To measure the surface pressure distributions, pressure taps were installed along the cylinder axis at 5-mm intervals and the cylinder was rotated in 10° increments in a counter-clockwise direction ($\theta$). The pressure taps were connected to a micro-manometer (FCO-12) and the analog pressure signals were digitized using a high-precision A/D converter (DT-2838), as shown in Fig. 1. At each measurement point, 16 384 pressure data were acquired using a sampling rate of 500 Hz after low-pass filtering at 200 Hz. A time delay of a few seconds was allowed before data sampling to allow the system time to recover from the pressure variations caused by channel scanning. The pressure difference between the surface pressure $p$ and the static pressure $p_0$ was divided by the dynamic pressure to give the pressure coefficient $C_p$, expressed as:

$$C_p = 2(p - p_0)/\rho_a U_0^2, \tag{6}$$

where the air density $\rho_a$ was determined from the measured air temperature with simply assuming dry air condition at the standard atmospheric pressure. It is important to note that the density depends on the temperature and humidity (Wylen et al., 1994). In this study, the partial vapor pressure or relative humidity in the air was not measured and the humidity effect was not considered. However, we maintained the air temperature almost constantly and carried out this experiment in winter season in which the humidity is usually very low. Therefore, the humidity effects embedded in the present results will be not so significant. Pressure data were measured around the entire periphery of the lower FC, because the presence of the adjacent cylinder causes the mean pressure distribution to be asymmetric with respect to the longitudinal axis.

## 3. Results and discussion

### 3.1. Flow visualization

The flow around a pair of $L/D = 6$ finite cylinders was visualized using a particle tracer method in a circulating water channel. The water channel was designed such that the oncoming flow had an ABL velocity profile that was nearly the same as that used for the wind tunnel experiments. Fig. 5 shows the flow visualized at mid-height of the cylinder for systems with various gap ratios in the range $1.0 \leqslant G/D \leqslant 2.0$. When there is no gap between the two cylinders ($G/D = 1.0$), the wake shows an asymmetric vortex structure and out-of-phase vortex-shedding. In this case, the FC models behave as a single bluff body.

As the gap ratio ($G/D$) increases, the gap flow passing through the gap between the two cylinders increases. This gap flow interacts actively with the vortex structure shed from the two cylinders and makes the near-wake unstable. Inspection of a time series of tracer particle images revealed that the flow passing through the gap seems to shift from periods of being biased towards one of the cylinders to periods in which it is biased towards the other cylinder. At the large gap ratio of $G/D = 2.0$, the flow pattern shows a nearly symmetric in-phase vortex structure without direct interaction between the inner shear layers developed from each cylinder. In this case, the gap flow is weakly deflected upwards or downwards. This gap ratio therefore represents a critical gap size, at which the out-of-phase vortex-shedding pattern changes into the in-phase vortex-shedding mode. This is in good agreement with previous results (Sumner et al., 1999).

Fig. 6 shows images of vertical cross-sections ($YZ$ plane) of the flow around the free ends of two finite cylinders for $G/D = 2.0$ taken at $X/D = 0$, 0.25 and 0.6. These cross-sections were illuminated with a thin light sheet and flow images were photographed from a downstream location. The oncoming flow accelerates in the region close to the free end of each cylinder, and then begins to roll-up from the cylinder circumference. A counter-rotating twin-vortex is observed above each FC free end. The left and right vortices of this twin-vortex rotate in clockwise and counter-clockwise directions, respectively. The two vortices are almost symmetric, but differ slightly in size. The size of the swirling vortices increases as the flow goes downstream, as shown in Fig. 6(b) and (c). The two vortices interfere with each other and the wake width increases as the flow goes downstream. It is interesting to note that as the flow moves downstream the thickness of the inner shear layer of each cylinder wake increases only slightly, whereas the outer shear layer expands substantially (Fig. 6(c)). This may be due to the fact that high-speed gap flow suppresses the development of inner shear layers and pushes the near-wake outwards.

Park and Lee (2000) found a peculiar flow structure with a 24 Hz frequency component that was closely related to the counter-rotating twin-vortex generated from a single FC free end. These two vortices of the peculiar flow structure have no phase difference, i.e., they are in phase in the near-wake. This peculiar frequency dominates in the region near the FC free end and is independent of the periodic vortex-shedding frequency. Kitagawa et al. (1999) also found that the

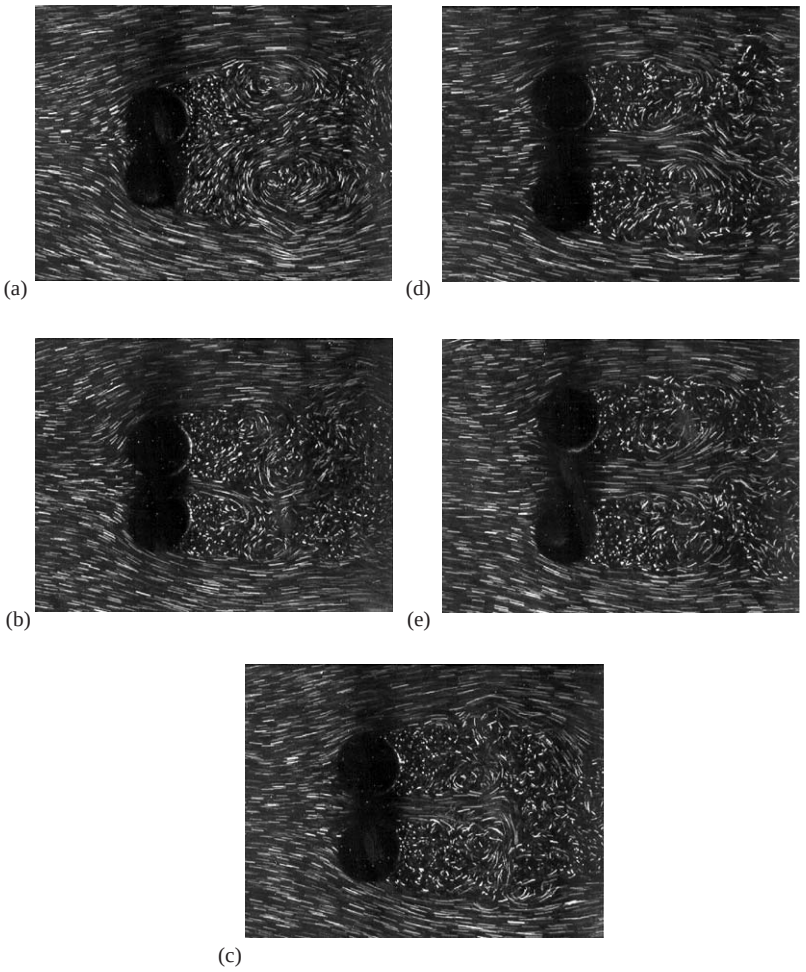


Fig. 5. Flow around a pair of $L/D=6$ cylinders visualized at $Z/L=0.5$; the effect of gap ratio ($G/D$): (a) $G/D=1.0$; (b) $G/D=1.25$; (c) $G/D=1.5$; (d) $G/D=1.75$; (e) $G/D=2.0$.

frequency of tip-associated vortices formed around the free end of a FC was lower than the Kármán vortex-shedding frequency.

Fig. 7 shows typical top views of the flow near the free ends of two finite cylinders for the gap ratio of $G/D=2.0$ at several heights. Flow images were captured by moving the horizontal light sheet downward from $Z/L=1.083$ to 0.875. The visualized flows are almost symmetric with respect to the symmetry axis and show in-phase vortex-shedding for all of the horizontal planes near the FC free ends.

On approaching the top of the FC ($Z/L=1.0$ and 0.958), the oncoming flow ascends in front of the FC free end and shows nearly uniform flow in the region above the free end ($Z/L=1.083$ and 1.042), with the exception of some fluctuations close to the edge of the free end (Fig. 7(a)–(d)). Thereafter, it starts to descend downward just behind the cylinder. Recirculation bubbles form on the top surface of the FC free end. After passing the back edge of each FC free end, the shear flow separated from the free end descends downward along the central wake region of the FC. The wake flow is highly turbulent due to active interaction between the descending shear layer from the FC free end and the entrained flow from both sides of each FC.

On moving further down the cylinder axis, the shear flow separated from the FC free end descends downward along the center-line of the wake as shown in Fig. 7(e) and (f). The vortex streets behind the finite cylinders expand and interfere with each other as the flow moves downstream. The length of the vortex formation region and the width of the wake formed behind the FC increase with going downward position along the cylinder axis. From these observations, we can conjecture that the delay of flow separation on both sides of the FC embedded in the ABL causes the vortex formation region and wake width to be smaller than those observed for a FC located in a uniform flow.

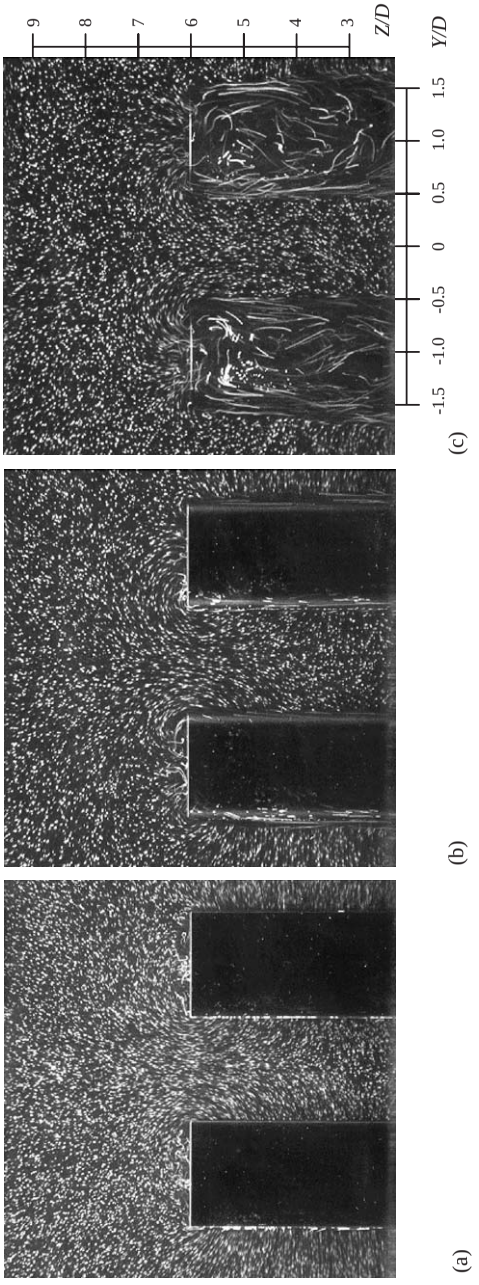


Fig. 6. Cross-sectional views of flow around the free ends of two finite cylinders for $G/D=2.0$: (a) $X/D=0$; (b) $X/D=0.25$; (c) $X/D=0.6$.

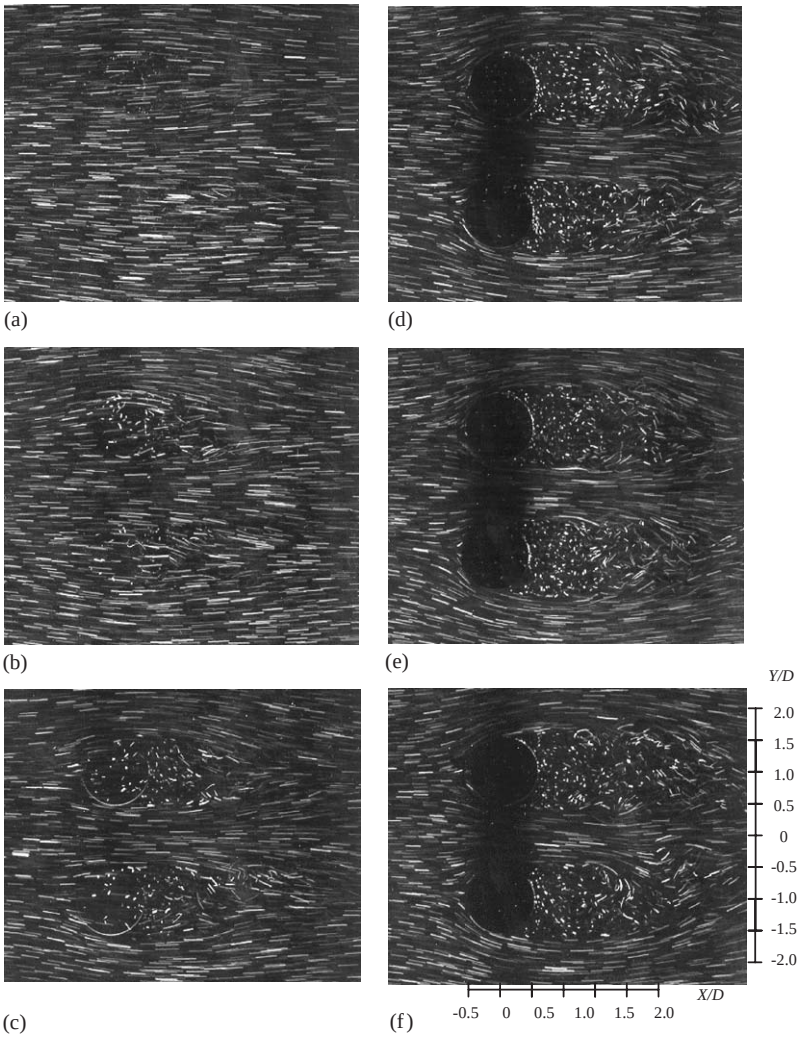


Fig. 7. Top views of visualized flow around the free ends of two finite cylinders at several heights ($G/D=2.0$): (a) $Z/L=1.083$; (b) $Z/L=1.042$; (c) $Z/L=1.0$; (d) $Z/L=0.958$; (e) $Z/L=0.917$; (f) $Z/L=0.875$.

### 3.2. *Vortex-shedding frequency*

Sumner et al. (1999) reported that the asymmetrical flow pattern observed at intermediate gap ratios is generally characterized by the formation of a narrow near-wake behind one cylinder, a wide near-wake behind the other cylinder, and two different vortex-shedding frequencies. In the present study, the velocity signals of the wake were analyzed to investigate the effect of gap ratio ($G/D$) on the vortex-shedding frequency ($f_s$). For a 2-D circular cylinder, the large-scale vortices shed from the two sides of the cylinder are almost uniform along the cylinder spanwise direction. However, the wake behind a finite cylinder with a free end is quite different from that behind a 2-D cylinder. In particular, the regular vortex-shedding observed from the 2-D cylinder is greatly influenced by the downwash flow separated from the FC free end. The separated shear flow influences the wake structure down to a certain vertical distance from the FC free end, such that its effect can be detected at the mid-height of FC models having small aspect ratio (Szepessy and Bearman, 1992; Park and Lee, 2000).

Fig. 8 shows power spectral density (PSD) distributions measured at the downstream location $X/D=2$, $y_U/D=1.5$ and $Z/L=0.5$ for various gap ratios. The vortex-shedding frequencies for the finite cylinders are smaller than that of a single 2-D cylinder ($f_s=66$ Hz, not shown here). The decrease in the vortex-shedding frequency seems to be related to the influx of ambient inviscid flow into the near-wake region due to the descending downwash flow. Since the PSD

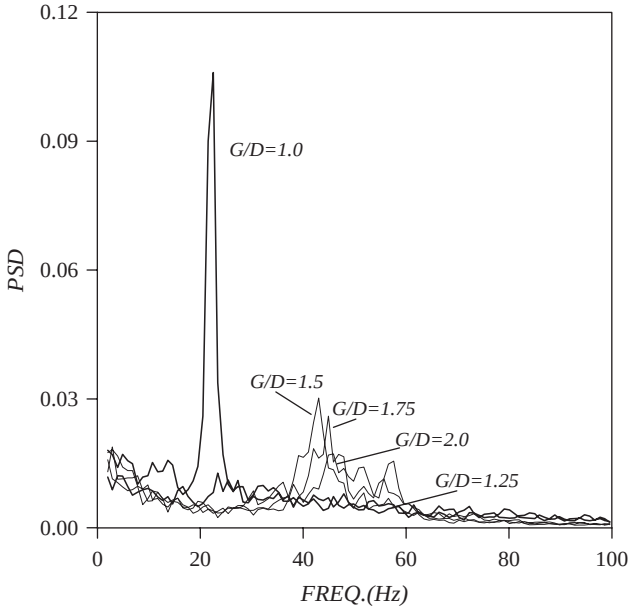


Fig. 8. Variation of vortex-shedding frequency measured at $X/D=2$, $y_U/D=1.5$ and $Z/L=0.5$.

distribution was measured at the mid-height of the cylinder, the effects of the wall boundary layer and horseshoe vortex on the vortex-shedding frequency can be assumed to be negligible.

At the small gap ratio of $G/D=1.25$, the value of the PSD is small at all frequencies and the distribution does not exhibit a clear peak. This may be due to the weak gap flow at this gap ratio, as shown in Fig. 5(b), and also to the fact that the vortices shed from the two cylinders are of similar magnitude, but are out of phase with each other. This difference in the phase causes the velocity fluctuations at the vortex-shedding frequency to cancel out and therefore the distribution does not show any dominant periodic feature. At the gap ratio of $G/D=1.0$, however, the 24 Hz frequency component dominates. These frequency characteristics seem to be related to the inflow of ambient inviscid fluid into the wake region due to flow separation from the FC free end. Price et al. (2002) found that the gap flow between a 2-D horizontal cylinder and the bottom wall was extremely weak and that no regular vortex-shedding occurred for small gap ratios in the range $G/D \leqslant 1.125$. They reported that the inner and outer shear layers of the cylinder wake were strongly dependent on the Reynolds number for small gap flow.

As the gap ratio increases above $G/D=1.25$, the PSD distribution begins to show a peak at the vortex-shedding frequency. This results from the gap flow passing with appreciable momentum, initiating vortex-shedding from both sides of each cylinder that leads to regular shedding of vortices from the inner shear layer. The peak frequency increases slightly with increasing gap ratio, with values of 43 Hz at $G/D=1.5$, 45 Hz at $G/D=1.75$, and 46 Hz at $G/D=2.0$. This increase in the frequency indicates that the Strouhal number ($\mathrm{St}=f_sD/U$) increases with increasing gap ratio, which is consistent with the results of previous studies (Spivack, 1946; Williamson, 1985). The Strouhal number for the two-cylinder arrangement increases up to the critical gap ratio regime, but changes little on further increase of the gap ratio between the two cylinders.

Fig. 9 shows the cross-correlation function ($R_{u_1u_2}$) between the velocity signals measured at the sides (upper cylinder: $y_U/D=+1.5$, lower cylinder: $y_L/D=-1.5$) of the two finite cylinders at $X/D=3$ and $Z/L=0.5$. Two single hot-wire probes were installed in parallel at the locations $y_U/D=+1.5$ and $y_L/D=-1.5$, and the velocity signals from the two probes were measured simultaneously. The velocity signals were band-pass-filtered in the range of $\pm 5$ Hz around the vortex-shedding frequency to observe the relationship between the wakes behind the two cylinders. When there is no gap between the two FC models ($G/D=1.0$), the cross-correlation function has a small positive value at no time delay ($\tau=0$). This indicates that a weak vortex-shedding with a small phase difference occurs from the two sides of the finite cylinders, which resembles the wake behind a single bluff body.

For gap ratios greater than $G/D=1.0$, the cross-correlation function shows a local minimum at $\tau=0$ (no time delay), indicating that the velocity signals measured at the two outer sides of the FC models are 180° out-of-phase. This phase difference results from the increase in the gap flow between the two cylinders, which leads to regular vortex-shedding for

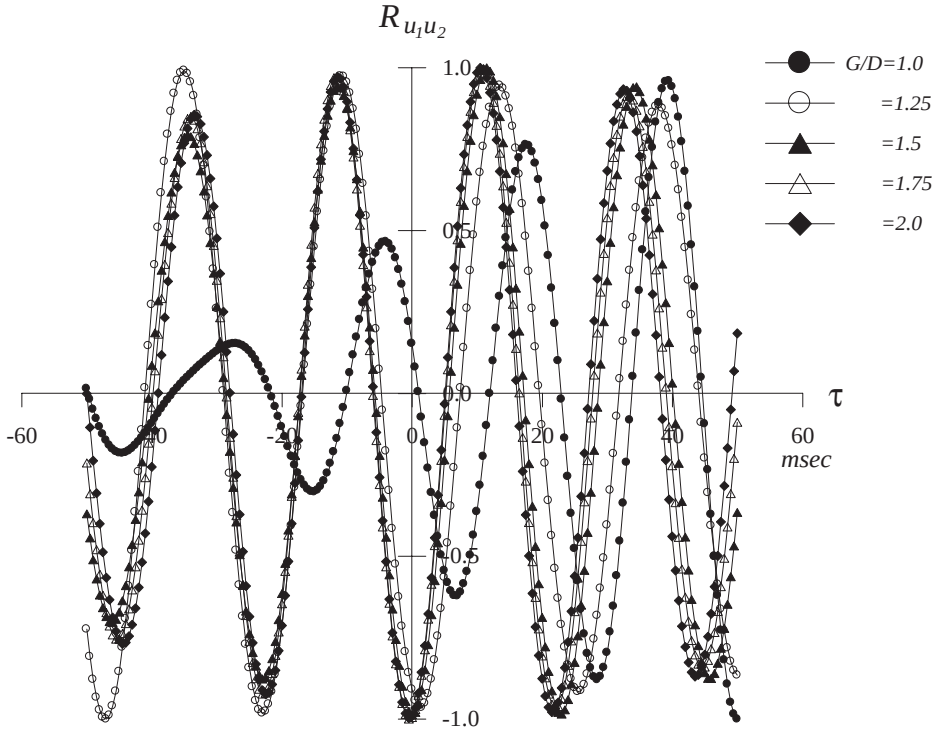


Fig. 9. Cross-correlation function of two velocity signals measured at both sides ($y_U/D = +1.5$, $y_L/D = -1.5$) of two cylinders at $X/D = 3$ and $Z/L = 0.5$.

each cylinder. This phenomenon is evident in the flow visualization results, especially at large gap ratios. Taken together, these results suggest that the wake of each FC is almost symmetric with respect to the wake center-line ($Y = 0$) without the active interaction between the two inner shear layers that occurs when there is gap flow.

### 3.3. Vortex formation region

The entrainment of ambient fluid into the wake region affects not only the wake structure but also the vortex formation behind the FC, as shown in Fig. 10. The wake velocities were measured along the wake center-line ($y_U/D = 0$) of the upper cylinder. The distance from the cylinder center to the location of the peak in the velocity fluctuations was used to determine the location at which the roll-up of the shear layer takes place. In this study, the end of the vortex formation region is defined as the point on the wake center-line at which the streamwise turbulence intensity is greatest. It is assumed that the transverse velocity component induced on each vortex is negligible and the convection velocity of vortices in the streamwise direction is the same (Bearman and Wadcock, 1973).

A single hot-wire probe was used to measure the length of the vortex formation region. Although hot-wire anemometry gives inaccurate results in a highly turbulent separated shear flow, several previous researchers have successfully measured the vortex formation region by detecting only the location of the peak in the streamwise velocity fluctuations (Szepessy and Bearman, 1992). The raw velocity signals measured along the wake center-line were band-pass-filtered at twice the vortex-shedding frequency with bandwidth of $\pm 5$ Hz to evaluate the length of vortex formation region. For the no-gap case ($G/D = 1.0$), the length of the vortex formation region is large, but the magnitude of the turbulence intensity is small. This behavior is attributed to the fact that at this gap ratio the two FC models behave as a single bluff body with a large frontal area. At the gap ratio of $G/D = 1.25$, the length of the vortex formation region has a minimum value [about one cylinder diameter downstream ($X/D = 1.5$)] due to the small amount of gap flow between the two finite cylinders (Price et al., 2002). For gap ratios greater than $G/D = 1.5$, the vortex formation region remains almost unchanged and the turbulence intensity at double the vortex-shedding frequency is large.

Fig. 11 shows the spatial distribution of streamwise turbulence intensity of raw velocity signals measured at the mid-height horizontal plane ($Z/L = 0.5$). The wake width is usually defined as the lateral distance between the two points

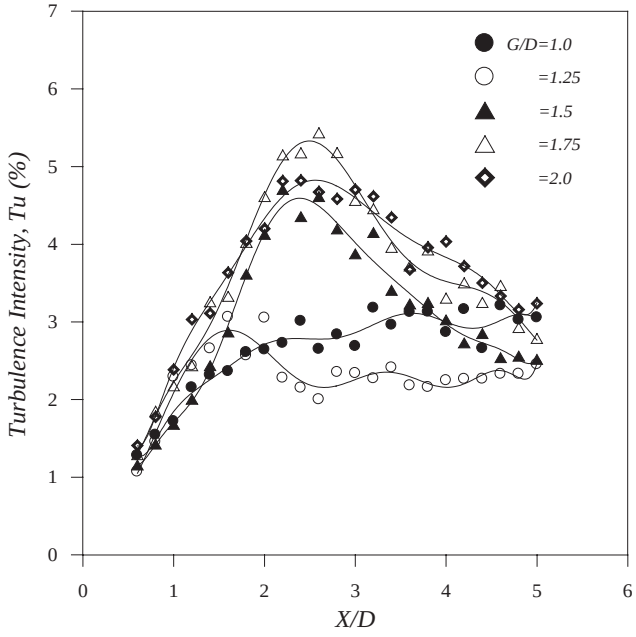


Fig. 10. Variation of turbulence intensity profiles at $y_U/D=0$ and $Z/L=0.5$.

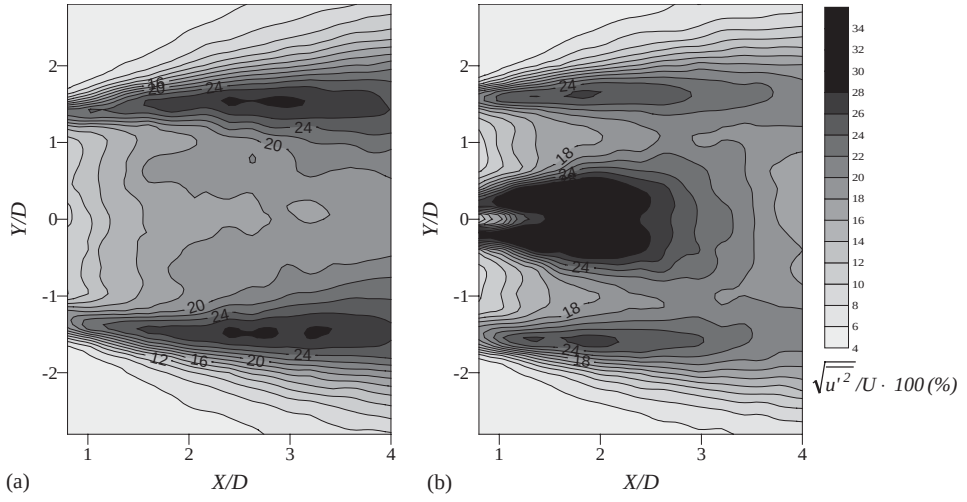


Fig. 11. Turbulence intensity distribution of streamwise velocity component at $Z/L=0.5$: (a) $G/D=1.0$; (b) $G/D=1.5$.

that have the maximum streamwise turbulence intensity. The shear layers separated from the two sides of each cylinder develop gradually as the flow goes downstream. From Fig. 11, we can see that the vortex formation region at the gap ratio of $G/D=1.5$ is much smaller than that for the no-gap case. The decrease in the size of the vortex formation region can be attributed to the recovery of regular vortex-shedding as the gap ratio increases. When there is no gap between the two cylinders ($G/D=1.0$), the streamwise turbulence intensity has small values along the axis of symmetry ($Y/D=0$) due to the lack of gap flow. The streamwise turbulence intensity gradually increases with going downstream along the center-line, as is observed for the wake of a single bluff body. This increase in turbulence results from the interaction of the vortices shed from the outer side of each cylinder and the descending downwash flow from the FC free end along the

wake center-line. At the gap ratio of $G/D=1.5$, however, the turbulence intensity is large at the wake center ($Y/D=0$) due to the high-speed gap flow. Although the spatial distribution of turbulence intensity is symmetric with respect to the wake center, it is worthwhile to note that the wake structure behind each FC model is not symmetric with respect to the center of each cylinder wake.

The mean velocity and turbulence intensity profiles of the streamwise velocity component at mid-height of the FC model measured with an X-type hot-wire probe at the downstream location of $X/D=4$ are compared in Fig. 12. The mean streamwise velocity is characterized by large velocity deficits in the central wake region, as shown in Fig. 12(a). The descending downwash flow induces a complicated three-dimensional wake structure behind the cylinders. As a result, the other two velocity components, $V$ and $W$ (not shown here), become dominant in the region near the FC free end and the velocity deficit of the streamwise velocity component is increased. For small gap ratios of $G/D=1.25$ and 1.5, the mean streamwise velocity is substantially lower in the gap region between the two FC models. At the gap ratio of $G/D=2.0$, the velocity deficit is largely recovered due to the increase in the speed of the gap flow along the axis of symmetry ($Y/D=0$).

Fig. 12(b) shows the streamwise turbulence intensity profiles measured at the same downstream location. At small gap ratios ($G/D=1.0$, 1.25, 1.5), the streamwise turbulence intensity profile exhibits a double peak similar to that

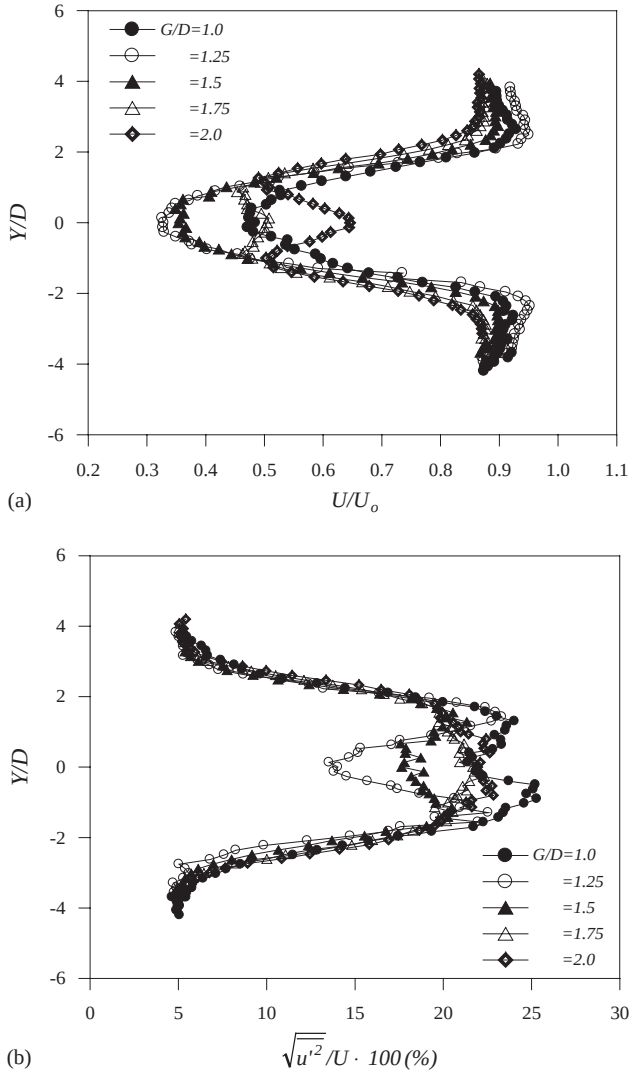


Fig. 12. Comparison of streamwise mean velocity and turbulence intensity profiles measured at $X/D=4$ and $Z/L=0.5$: (a) mean velocity; (b) turbulence intensity.

observed for a 2-D circular cylinder. In particular, for the gap ratio of $G/D=1.25$, the turbulence intensity has a local minimum in the gap region. As the gap ratio increases, however, the profile takes on a parabolic shape with a single peak at the wake center. This indicates that the coherent vortical structure formed behind each cylinder interacts actively with the downwash in the central gap region, increasing the streamwise turbulence intensity.

### 3.4. Surface pressure

Fig. 13 shows the effect of gap ratio ($G/D$) on the surface pressure distribution around the lower FC model at mid-height ($Z/L=0.5$). The mean pressure distribution is not symmetric with respect to the center-line of the cylinder due to presence of the adjacent cylinder. The location of the actual stagnation point shifts about 10° toward the inner windward region ($\theta=350°$) due to creation of a gap between the two cylinders in comparison to a single 2-D cylinder case. As the oncoming flow accelerates along the cylinder surface from the geometric stagnation point ($\theta=0°$), the surface pressure on the outer windward surface rapidly decreases. As the gap ratio ($G/D$) increases, the mean pressure on the outer windward surface ($0°<\theta<90°$) increases. This indicates that as the gap ratio is reduced, the increase in the blocking of the oncoming flow in the gap region causes an increase in the flow speed above the outer windward surface.

On the leeward surface ($90°<\theta<270°$), the mean pressure is nearly uniform irrespective of the gap ratio. For the no-gap case ($G/D=1.0$), the mean pressure on the inner windward side ($270°<\theta<360°$) is almost uniform due to the accumulation of the approaching flow near the stagnation point. As the gap ratio increases, however, the mean pressure on the inner windward surface decreases due to the increased gap flow between the two FC models.

Fig. 14 shows the mean pressure distributions on the cylinder surface near the FC free end for the gap ratio of $G/D=1.5$. Since the atmospheric boundary layer has a vertical velocity gradient, the mean pressure at the stagnation point ($\theta=350°$) decreases with decreasing vertical position along the cylinder axis from the FC free end. The mean pressure on the outer windward surface in the region near the FC free end decreases more rapidly than that in the mid-height region. This is attributed to the descending downwash flow near the free end and the entrainment of ambient fluid.

On the leeward cylinder surface ($90°<\theta<270°$), the mean pressure decreases with approaching the FC free end. This low pressure on the leeward surface of the cylinder is closely related to the descending shear flow separated from the FC free end. The mean pressure distribution on the inner leeward side ($180°<\theta<270°$) shows a trend similar to that of the outer leeward surface ($90°<\theta<180°$). However, the mean pressure on the inner leeward side is on the substantial decrease in comparison to the outer leeward surface case on approaching the top of the FC. With decreasing vertical position along the cylinder axis from the FC free end, the regular vortices shed from the two sides of each cylinder become dominant and the effect of the descending shear layer weakens. This indicates that the mean pressure on the

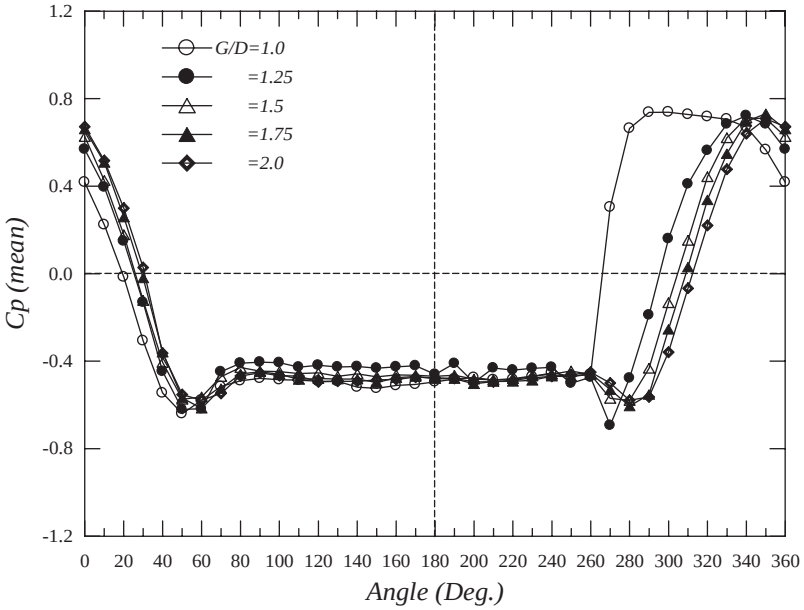


Fig. 13. Comparison of mean pressure distributions at $Z/L=0.5$.

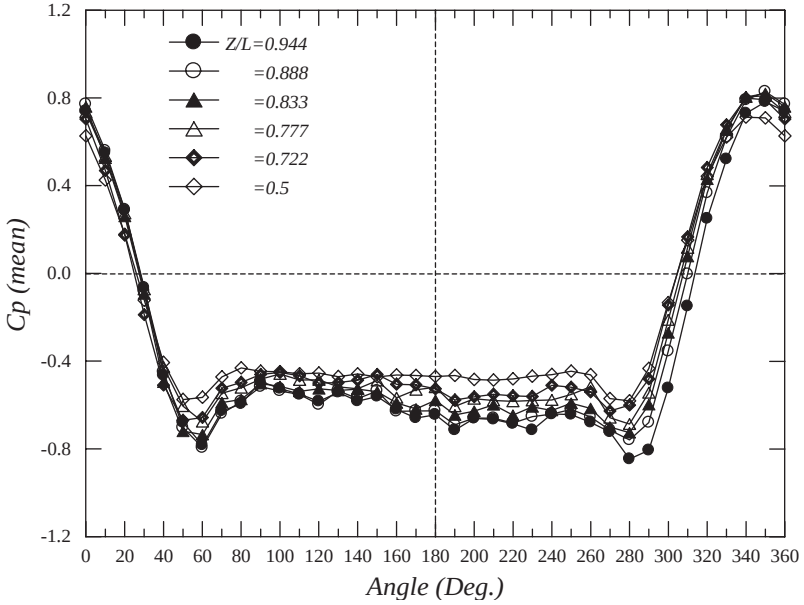


Fig. 14. Mean pressure distributions near the *FC* free end for the gap ratio of $G/D = 1.5$.

leeward cylinder surface increases with moving downward position along the cylinder axis by recovering the mean base pressure.

## 4. Conclusions

The flow structure around the free-end region of two adjacent finite circular cylinders embedded in an atmospheric boundary layer (ABL) was investigated experimentally. Systems with gap ratios in the range 1.0 to 2.0 were investigated. The flow fields were measured using hot-wire anemometry and the wake structure was visualized using a particle tracer method. The wake flow behind a finite cylinder (FC) was found to be markedly different from that behind a general 2-D cylinder. When a fluid flows past a FC, the strong entrainment of ambient irrotational fluids due to the counter-rotating twin vortices separated from the FC free end leads to the formation of a three-dimensional wake. In addition, the flow structure around two adjacent finite cylinders is more complicated than that around a single cylinder due to mutual interference. In contrast to the uniform flow condition, under ABL flow conditions the streamwise mean velocity profiles have a velocity gradient in the vertical direction and the turbulence intensity is increased. Both the vortex-shedding frequency and vortex formation length are decreased for finite cylinders embedded in an ABL due to the delay of flow separation.

When the two FC models are in contact ($G/D = 1.0$), the wake structure is asymmetric because the two cylinders behave as a single bluff body. As the gap ratio is increased to values greater than $G/D = 1.25$, the flow passing through the gap between the two cylinders increases and the velocity deficit in the center region of the wake is recovered due to increased speed of the gap flow. This gap flow actively interacts with the vortices shed from the two cylinders. The gap flow seems to shift from periods of being biased towards one cylinder to periods of being biased towards the other cylinder. At the large gap ratio of $G/D = 2.0$, the flow exhibits an almost symmetric in-phase shedding pattern without direct interaction between the two inner shear layers of the wakes behind each FC. The gap flow is weakly deflected upwards or downwards before the rolling-up of vortices. When there is a gap between the two FC models, the vortex formation region formed behind each cylinder is smaller than that for the no-gap case.

The mean pressure distribution on the FC surface is not symmetric with respect to the center-line of each cylinder and the stagnation point is shifted about 10° toward the inner windward region due to the presence of the adjacent cylinder. The mean pressure at the stagnation point decreases with decreasing vertical position along the cylinder axis from the FC free end due to the vertical velocity gradient of ABL flow. The mean pressure on the FC leeward surface decreases on approaching the FC free end.

**Acknowledgement**

The authors thank the supports of NRL (National Research Laboratory) program of the Ministry of Science and Technology, Korea.

**References**

Baban, F., So, R.M.C., 1991. Aspect ratio effect on flow-induced forces on circular cylinders in a cross-flow. Experiments in Fluids 10, 313–321.

Bearman, P.W., Wadcock, A.J., 1973. The interaction between a pair of circular cylinders normal to a stream. Journal of Fluid Mechanics 61, 499–511.

Castro, I., Robins, A., 1977. The flow around a surface-mounted cube in uniform and turbulent systems. Journal of Fluid Mechanics 79, 307–335.

Farivar, D., 1981. Turbulent uniform flow around cylinders of finite length. American Institute of Aeronautics and Astronautics Journal 19 (3), 275–281.

Fox, T.A., Apelt, C.J., West, G.S., 1993. The aerodynamic disturbance caused by the free-ends of a circular cylinder immersed in a uniform flow. Journal of Wind Engineering and Industrial Aerodynamics 49, 389–400.

Kitagawa, T., Fujino, Y., Kimura, K., 1999. Effects of free-end condition on end-cell-induced vibration. Journal of Fluids and Structures 13, 499–518.

Mahir, N., Rockwell, D., 1996. Vortex formation from a forced system of two cylinders. Part II: side-by-side arrangement. Journal of Fluids and Structures 10, 491–500.

Okamoto, S., Sunabashiri, Y., 1992. Vortex-shedding from a circular cylinder of finite length placed on a ground plane. Journal of Fluids Engineering 114, 512–521.

Park, C.W., Lee, S.J., 2000. Free end effects on the near-wake flow structure behind a finite circular cylinder. Journal of Wind Engineering and Industrial Aerodynamics 88, 231–246.

Park, C.W., Lee, S.J., 2002. Flow structure around a finite circular cylinder embedded in various atmospheric boundary layers. Fluid Dynamics Research 30, 197–215.

Price, S.J., Sumner, D., Smith, J.G., Leong, K., Paidoussis, M.P., 2002. Flow visualization around a circular cylinder near to a plane wall. Journal of Fluids and Structures 16, 175–191.

Sakamoto, H., Arie, M., 1983. Vortex-shedding from a rectangular prism and a circular cylinder placed vertically in a turbulent boundary layer. Journal of Fluid Mechanics 126, 147–165.

Sayers, A.T., 1988. Flow interference between four equispaced cylinders when subjected to a cross flow. Journal of Wind Engineering and Industrial Aerodynamics 31, 9–28.

Simiu, E., Scanlan, R.H., 1996. Wind Effects on Structures. Wiley, New York, pp. 46–64.

Sitheeq, M.M., Iyengar, A.K.S., Farell, C., 1997. Effect of turbulence and its scales on the pressure field on the surface of a three-dimensional square prism. Journal of Wind Engineering and Industrial Aerodynamics 69–71, 461–471.

Slaouti, A., Gerrard, J.H., 1981. An experimental investigation of the end effects on the wake of a circular cylinder towed through water at low reynolds numbers. Journal of Fluid Mechanics 112, 297–314.

Spivack, H.M., 1946. Vortex frequency and flow pattern in the wake of two parallel cylinders at varied spacing normal to an air stream. Journal of Aeronautical Sciences 13, 289–297.

Sumner, D., Wong, S.S.T., Price, S.J., Paidoussis, M.P., 1999. Fluid behavior of side-by-side circular cylinders in steady cross-flow. Journal of Fluids and Structures 13, 309–338.

Sun, T.F., Gu, Z.F., He, D.X., Zhang, L.L., 1992. Fluctuating pressure on two circular cylinders at high reynolds numbers. Journal of Wind Engineering and Industrial Aerodynamics 41–44, 577–588.

Szepessy, S., Bearman, P.W., 1992. Aspect ratio and end plate effects on vortex-shedding from a circular cylinder. Journal of Fluid Mechanics 234, 191–217.

Uematsu, Y., Yamada, M., Ishii, K., 1990. Some effects of free-stream turbulence on the flow past a cantilevered circular cylinder. Journal of Wind Engineering and Industrial Aerodynamics 33, 43–52.

West, G.S., Apelt, C.J., 1982. The effects of tunnel blockage and aspect ratio on the mean flow past a circular cylinder with reynolds numbers between $10^4$ and $10^5$. Journal of Fluid Mechanics 114, 361–377.

Williamson, C.H.K., 1985. Evolution of a single wake behind a pair of bluff bodies. Journal of Fluid Mechanics 159, 1–18.

Williamson, C.H.K., 1989. Oblique and parallel modes of vortex-shedding in the wake of a circular cylinder at low reynolds numbers. Journal of Fluid Mechanics 206, 579–627.

Wylen, G.J.V., Sonntag, R.E., Borgnakke, C., 1994. Fundamentals of Classical Thermodynamics. Wiley, New York, pp. 491–533.